2019

Synthesis of methotrexate-loaded tantalum pentoxide-poly(acrylic acid) nanoparticles for controlled drug release applications

Kathrin Bogusz
University of Wollongong, kb543@uowmail.edu.au

Malgorzata Zuchora
University of Wollongong, miz996@uowmail.edu.au

Vitor Sencadas
University of Wollongong, victors@uow.edu.au

Moeava Tehei
University of Wollongong, moeava@uow.edu.au

Michael L. F Lerch
University of Wollongong, mlerch@uow.edu.au

See next page for additional authors

Publication Details

Bogusz, K., Zuchora, M., Sencadas, V., Tehei, M., Lerch, M., Thorpe, N., Rozenfeld, A., Dou, S. Xue., Liu, H. Kun. & Konstantinov, K. (2019). Synthesis of methotrexate-loaded tantalum pentoxide-poly(acrylic acid) nanoparticles for controlled drug release applications. Journal of Colloid and Interface Science, 538 286-296.

Synthesis of methotrexate-loaded tantalum pentoxide-poly(acrylic acid) nanoparticles for controlled drug release applications

Abstract
Over the past decade, there has been increasing interest in the use of multifunctional nanoparticles (NPs) for cancer treatment. Of importance are systems that can deliver drugs at a sustained rate to target cancer cells, which can result in higher efficiency and reduced systemic toxicity. In this study, we present the route for the synthesis of tantalum pentoxide (Ta_2O_5) NPs with a particle size of 27 nm that were individually coated with poly(acrylic acid) (PAA) with a different layer thickness of 2-8 nm by in-situ polymerization of the acrylic acid monomer. The capability of Ta_2O_5-PAA to provide anatomical contrast-enhancing features has been demonstrated via computed tomography. The Ta_2O_5-PAA conjugate was further loaded with methotrexate, and the drug release was observed for a total of 72 h at a pH of 3.6, 5.4, 7.4, and 9.4. While the different layer thicknesses did not influence the drug release kinetics, a decrease in pH of the release medium resulted in a slower drug release. The developed nanocomposite particles present a great potential as a theranostic system for biomedical applications.

Disciplines
Medicine and Health Sciences

Publication Details
Bogusz, K., Zuchora, M., Sencadas, V., Tehei, M., Lerch, M., Thorpe, N., Rozenfeld, A., Dou, S. Xue., Liu, H. Kun. & Konstantinov, K. (2019). Synthesis of methotrexate-loaded tantalum pentoxide-poly(acrylic acid) nanoparticles for controlled drug release applications. Journal of Colloid and Interface Science, 538 286-296.

Authors
Kathrin Bogusz, Malgorzata Zuchora, Vitor Sencadas, Moeava Tehei, Michael L. F Lerch, Nathan Thorpe, Anatoly B. Rosenfeld, Shi Xue Dou, Hua-Kun Liu, and Konstantin K. Konstantinov

Synthesis of Methotrexate-Loaded Tantalum Pentoxide–Poly(Acrylic Acid) Nanoparticles for Controlled Drug Release Applications

Kathrin Bogusz[a,b], *Malgorzata Zuchora*[a,b], *Vitor Sencadas*[c,d]*, *Moeava Tehei*[b,e], *Michael Lerch*[e,f], *Nathan Thorpe*[e], *Anatoly Rosenfeld*[b,e], *Shi Xue Dou*[a], *Hua Kun Liu*[a], *and Konstantin Konstantinov*[a,b,]*

[a] Institute for Superconducting and Electronic Materials, Australian Institute for Innovative Materials, University of Wollongong, NSW 2522, Australia.

[b] Illawarra Health and Medical Research Institute, University of Wollongong, NSW 2522, Australia.

[c] School of Mechanical, Materials, Mechatronics and Biomedical Engineering, Faculty of Engineering and Information Science, University of Wollongong, NSW 2522, Australia.

[d] ARC Center of Excellence for Electromaterials Science, University of Wollongong, NSW 2522, Australia.

[e] Centre for Medical Radiation Physics, Faculty of Engineering and Information Science, University of Wollongong, NSW 2522, Australia.

Corresponding Author

*Vitor Sencadas: victors@uow.edu.au, vsencadas@gmail.com

*Konstantin Konstantinov: konstan@uow.edu.au

KEYWORDS: theranostic system, anatomical contrast, controlled drug release, poly(acrylic acid), Ta_2O_5 nanoparticles, methotrexate, pH-responsive

ABSTRACT

Over the past decade, there has been increasing interest in the use of multifunctional nanoparticles (NPs) for cancer treatment. Of importance are systems that can deliver drugs at a sustained rate to target cancer cells, which can result in higher efficiency and reduced systemic toxicity. In this study, we present the route for the synthesis of tantalum pentoxide (Ta_2O_5) NPs with a particle size of 27 nm that were individually coated with poly(acrylic acid) (PAA) with a different layer thickness of 2 – 8 nm by in-situ polymerization of the acrylic acid monomer. The capability of Ta_2O_5-PAA to provide anatomical contrast-enhancing features has been demonstrated via computed tomography. The Ta_2O_5-PAA conjugate was further loaded with methotrexate, and the drug release was observed for a total of 72 h at a pH of 3.6, 5.4, 7.4, and 9.4. While the different layer thicknesses did not influence the drug release kinetics, a decrease in pH of the release medium resulted in a slower drug release. The developed nanocomposite particles present a great potential as a theranostic system for biomedical applications.

INTRODUCTION

At present, cancer is still one of the leading causes of death worldwide. While classical cancer therapies such as surgery, chemotherapy, and radiation therapy are typically based on the removal of malignant tissue, new approaches try to improve anticancer treatments by combining multiple features on a single platform [1, 2]. These so-called theranostic systems consist of therapeutic, targeting, and diagnostic agents, which can also act as radiation-dose enhancing agents that can reduce the overall radiation dosage [3]. In particular, the use of nanoparticles (NPs) is of interest, since they navigate easily across various biological barriers to preferentially accumulate in tumor tissues due to their enhanced permeability and retention effects [4].

Ta_2O_5 is a transition metal oxide that can be synthesized by precipitation routes with subsequent annealing [5]. Furthermore, Ta_2O_5 is chemically inert [6], biocompatible [7], shows good radiopacity [8], and is nearly insoluble, except for very strong bases and hydrofluoric acid [9, 10]. Due to the high atomic number of Ta (Z = 73) and density of 16.6 g/cm^3, Ta_2O_5 NPs have been investigated for their ability to increase anatomical contrast [6, 11, 12], as well as the induction of dose enhancement on radioresistant 9L rat gliosarcoma cancer cells in an megavoltage (MV) photon field [5]. *In vitro* studies showed that at equal molar concentrations of tantalum and iodine, the image contrast was larger with tantalum across the diagnostic X-ray spectrum [6]. Another advantage of the use of NPs, and in particular Ta_2O_5 ones, is their facile modifiable surface and capability of loading with anti-cancer drugs, which is typically achieved with conjugation or encapsulation by a polymer layer [13]. These core-shell structures can further be of benefit for computed tomography (CT) imaging as they can be administrated intravenously and display subsequent renal clearance [6, 14].

The study of polymers for personalized medicine has been of increasing interest. On the nanoscale, polymers can improve the half-life, solubility, and stability of drug delivery systems, while reducing potential unpleasant chemotherapeutic side effects [15-17].

Poly(acrylic acid) (PAA) is a bio-adhesive polymer and does not require further treatment after insertion into the body [18, 19]. PAA is a biocompatible hydrophilic polymer that is a common component of hydrogels and can retain large amounts of water in its three-dimensional network [18]. Moreover, the shrinking and expansion of PAA depend on the pH value: an alkaline environment leads to swelling of PAA, while acidic conditions cause shrinking of the polymer [20].

Common chemotherapeutic drugs that can be attached to the NPs include doxorubicin (DOX), 5-fluorouracil (5-FU), and methotrexate (MTX). It was reported that mesoporous silica nanoparticles functionalized with polyethylene glycol succinate [21] or glycoprotein small interfering and a polydopamine outer layer [22] loaded with DOX showed to have a pH-sensitive release. The DOX molecules behave as pH and thermal responsive due to the pH-cleavage DOX gatekeeper in the mesoporous silica nanocore.

MTX is an antineoplastic agent used not only in cancer treatment (breast, leukemia, lymphoma, lung, osteosarcoma and bladder neoplasms) but also for autoimmune disorders such as rheumatoid arthritis and ectopic pregnancies [23]. Furthermore, MTX possesses a higher affinity to dihydrofolate reductase (DHFR) than folates, binding competitively to DHFR to inhibit DNA, RNA, and protein synthesis inside malignant cells. Since cancer cells characteristically have an overexpression of folate receptors on their surfaces, MTX can potentially offer a targeting feature [23-25].

In the clinical applications, high doses of MTX are often used ($\geq$ 500 mg/m^2) and administered intravenously in cycles within a single day, which is extremely painful for the patient. Hence, the development of controllable drug release delivery systems is required, to not only reduce the dosage frequency but also to decrease systemic toxicity [26], improving the patient overall life quality.

In general, there are two methods to load hydrogels as drug carriers. In the first method, the drug is added to the monomer mixture during the polymerization, which allows trapping of the drug within the polymer matrix. Since the conditions for the polymerization may have deleterious effects on the drug properties, this method is not always favored [27]. In the second approach, the hydrogel is placed in a solution containing the drug and allowed to swell until equilibrium is reached [27-30].

This work shows a route that uses the high surface area available in individual Ta_2O_5 nanoparticles to polymerize a nanometric layer of PAA, by applying different polymerization times ranging from 1 – 5 h. The evolution of the polymer layer with the polymerization time was assessed and further correlated with the loading capacity of MTX that was measured by swelling of the hydrogel in the drug solution at pH 7.4. The drug release of MTX was studied at different pH values, ranging from 3.6 up to 9.4 for a total of 72 h, and the released kinetics were systematically studied. The method thus developed opens a new approach to create novel theranostic system for advanced cancer therapy treatments.

MATERIALS AND METHODS

Synthesis of Ta_2O_5 NPs: The tantalum pentoxide NPs were synthesized using a classical precipitation route. First, 10 g (24.62 mmol) of tantalum ethoxide (≥ 99.98%, Sigma-Aldrich) was transferred carefully with the exclusion of water into 200 mL of ethanol (≥ 99.8%, Sigma-Aldrich). The solution was stirred at room temperature, and then 60 mL of deionized water was added quickly to the reaction mixture, which resulted in the formation of a white precipitate. The precipitate was filtered via centrifugation (Eppendorf), washed twice with deionized water, and dried at 90 °C overnight. To obtain crystalline Ta_2O_5, the precipitate was annealed in a tube furnace (LABEC) at 730 °C for 30 minutes under atmospheric conditions.

Coating of Ta_2O_5 NPs with PAA: The coating of Ta_2O_5 NPs with PAA was performed in three steps. First, 330 mg of Ta_2O_5 NPs was added into a centrifuge tube containing 25 mL of methanol (≥ 99.8%, Sigma-Aldrich). The centrifuge tube was placed in a sonication bath (Branson 3800, Ultrasonics Corp) and sonicated for 25 min. Then, the suspension was centrifuged, the NPs were resuspended in 20 mL of concentrated hydrochloric acid (37%,

Sigma-Aldrich), and the suspension was stirred gently under nitrogen (N_2) flow for 25 min. The suspension was centrifuged, and the NPs were resuspended in 20 mL of AA (99%, Sigma-Aldrich) and placed back under N_2-flow. The suspension was stirred for a total of 1, 2.5, and 5 h, respectively, at a temperature of 80 ± 1°C. After the desired amount of time, 10 mL of chloroform (≥ 99%, Sigma-Aldrich) was added to the reaction mixture to stop the polymerization process. The suspension was then centrifuged, washed three times with chloroform, and the coated NPs were dried at room temperature for 48 h.

To determine the surface properties of the Ta_2O_5 after treatment with HCl, an aliquot was taken before the resuspension in AA, washed three times with methanol, and dried at room temperature for 48 h.

Materials Characterization: The crystalline state of the materials was investigated using an Enhanced Mini-Materials Analyzer (EMMA) X-Ray Diffractometer from GBC Scientific. The measurements were carried out at room temperature with Cu Kα radiation (λ = 1.5418 Å) at 40 kV and 25 mA in the range of 20 to 80° at a rate of 2.00°/min with a step size of 0.02°. The mean crystallite size was calculated using the Scherrer equation:

$$d = \frac{K\lambda}{\beta\cos(\theta)} \qquad (1)$$

where d, K, λ, β, and θ is the average crystallite size, a constant (K = 0.89 for spherical particles), the wavelength of the X-ray radiation, the full width at half maximum, and the Bragg angle of diffraction, respectively.

Particle sizes and core-shell structures of the uncoated and coated samples were examined using a JEOL 7500 field emission scanning electron microscope (FESEM) and a JEOL JEM-2010 transmission electron microscope (TEM). A suspension of 0.5 mg/mL of the NPs in 2-propanol (≥ 99.5%, Sigma-Aldrich) was prepared and sonicated for 30 min, and one droplet was placed on

an LC 200-CU lacey/carbon 200 mesh copper grid. To acquire SEM images, an accelerating voltage of 5 kV with a working distance of 10 mm and a spot size of 10 was used. TEM images were acquired at an accelerating voltage of 200 kV.

Fourier-transform infrared spectroscopy (FTIR) was recorded on an IR Prestige 21 spectrometer (Shimadzu) between 4000 to 600 cm^{-1} via attenuated total reflectance ATR) using the MIRacle attachment and the number of scans was fixed to 64 with a resolution of 4 cm^{-1}.

The surface composition of Ta_2O_5 NPs, both after their treatment with HCl and after polymerization with AA was evaluated via XPS using a SPECS PHOIBOS 100 Analyzer installed in a high vacuum chamber with base pressure below 10^{-8} mbar. X-ray excitation was provided by Al Kα radiation with a photon energy of 1486.6 eV at a voltage of 12 kV and power of 120 W. The XPS binding energy spectra were recorded with a pass energy of 20 eV in fixed analyzer transmission mode, and the data analysis was carried out using CasaXPS v2.3.15 software.

The stability of the Ta_2O_5-PAA NPs was determined via TGA using a Mettler Toledo TGA/DSC 1 STAR-e system. Each sample was placed in an aluminum oxide pan and heated from 50 – 800°C at a heating rate of 5°C/min under air atmosphere.

Computed Tomography: The anatomical contrast enhancement capabilities of Ta_2O_5 NPs and the Ta_2O_5-PAA nanocomposite synthesized with the highest polymerization time was demonstrated using CT. Suspensions with concentrations of Ta ranging from 0 to 8 mg/mL in PBS were prepared in 1.5 mL vials and sonicated for 2 h. Then, the vials were imaged together using a Toshiba Asteion (model TSX-021A) whole body X-ray CT scanner with a tube voltage of 100, 120, and 135 kV. The CT images were obtained using the standard patient image reconstruction algorithms included with the scanner.

Swelling Studies: The swelling studies were conducted in buffer solutions with a pH of 3.6, 5.4, 7.4, and 9.4 at 37 °C. First, the weighted mass of the dry Ta_2O_5-PAA NPs (W_0) was added into the buffer solution with the desired pH value. At predetermined time intervals, the NPs were removed from the swelling medium, blotted with filter paper to remove excess buffer solution from the NP surfaces, and the weight of the swollen composite (W_1) was determined. The swelling behavior of the composites was observed for a total of 48 h, and the swelling ratio (*SR*) was then calculated [28]:

$$SR = \frac{(W_1 - W_0)}{W_0} \qquad (2)$$

In Vitro Drug Loading: For each polymerization time, a sample mass of 200 mg of Ta_2O_5-PAA NPs was added to 20 mL of a solution of 10 mg/mL MTX (≥ 98%, Sigma-Aldrich) in PBS. The soaked NPs were rinsed with PBS and dried under vacuum until the weight remained constant. The loading capacity was calculated according to:

$$\text{Loading capacity (\%)} = \frac{\text{The weight of the entrapped drug}}{\text{The weight of dry composite}} * 100 \qquad (3)$$

The entrapment efficiency was determined by:

$$\text{Entrapment efficiency (\%)} = \frac{\text{The weight of the entrapped drug}}{\text{The weight of drug used for entrapment}} * 100 \qquad (4)$$

In Vitro Drug Release Studies: To study the release profiles for the MTX-loaded Ta_2O_5-PAA NPs, 10 mg of the dry MTX-loaded NPs was added into glass vials, to which 10 mL of release

medium (buffer) was added. The release medium varied in pH value (pH: 3.6, 5.4, 7.4, and 9.4). The vials were placed on an orbital shaker at a rotation rate of 50 rpm and a constant temperature of 37 ± 1 °C. After predetermined time intervals (0, 15, 30, 45 min, and 1, 2, 6, 12, 24, and 72 h), 5 mL aliquots were taken for further quantification. UV-vis spectroscopy was used to determine the concentration of MTX present in the supernatant at a wavelength of 303 nm [31]. The absorbance was recorded on a UV-3600 spectrophotometer from Shimadzu over the range of 800 to 200 nm by using quartz cuvettes (optical path of 10 mm).

The concentration of MTX was determined by the Beer-Lambert law, and a calibration curve was established with known concentrations of MTX solutions:

$$A = c\varepsilon l \qquad (5)$$

where A is the absorbance, c is the concentration of the compound in solution, ε is the extinction coefficient, and l is the path length of the sample. The total amount of soaked MTX was estimated by centrifugation of the 72 h sample at 5000 rpm for 10 min. The remaining pellet was suspended in 0.1 M sodium hydroxide (NaOH, Sigma-Aldrich), as MTX is highly soluble in 0.1 M NaOH, and sonicated for 1 h. Then, methanol (Sigma-Aldrich) was added to the solution, which was sonicated for an additional 1 h [31].

RESULTS AND DISCUSSION

Nanocomposite particles crystallinity and morphology: X-Ray diffraction (XRD) was used to determine the crystalline phase of the Ta_2O_5 NPs before and after PAA polymerization onto the surface of the NPs. The obtained diffraction patterns (Figure 1a) show the presence of a single δ hexagonal phase with a crystallite size (calculated through the Scherrer equation) of 26.7 ± 5.4

nm, with all reflections matching the JCPDS card no. 19-1299. Furthermore, the coating of Ta_2O_5 with PAA preserves the crystalline phase of the ceramic nanoparticles.

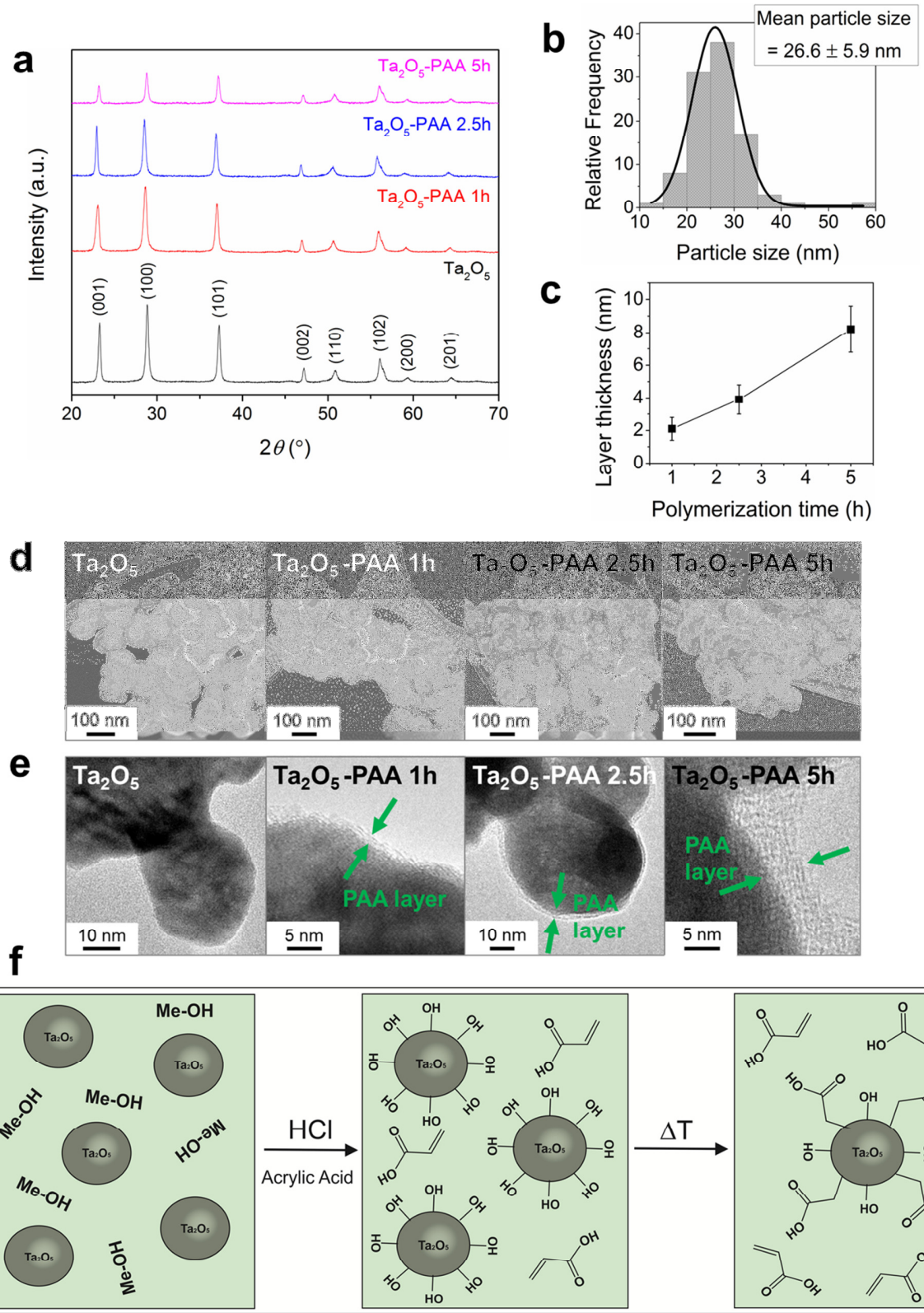
a
Ta2O5-PAA 5h
Ta2O5-PAA 2.5h
Ta2O5-PAA 1h
Ta2O5
(001)
(100)
(101)
(002)
(110)
(102)
(200)
(201)
Intensity (a.u.)
2θ (°)
b
Mean particle size
= 26.6 ± 5.9 nm
Relative Frequency
Particle size (nm)
c
Layer thickness (nm)
Polymerization time (h)
d
Ta2O5
Ta2O5-PAA 1h
Ta2O5-PAA 2.5h
Ta2O5-PAA 5h
100 nm
e
Ta2O5
Ta2O5-PAA 1h
Ta2O5-PAA 2.5h
Ta2O5-PAA 5h
PAA layer
10 nm
5 nm
f
Me-OH
HCl
Acrylic Acid
ΔT

Figure 1. a) XRD patterns of Ta_2O_5 NPs and Ta_2O_5-PAA nanocomposites with polymerization times of 1, 2.5, and 5 h, b) Particle size distribution of uncoated Ta_2O_5 NPs (a total of 100 particles were measured, and the relative frequency was plotted as a function of particle size), c) The plot of the layer thickness as a function of the polymerization time, d) SEM and e) TEM images of Ta_2O_5 NPs and Ta_2O_5-PAA nanocomposites with polymerization times of 1, 2.5, and 5 h. The green arrows indicate the PAA layers, and f) The expected reaction for the as-prepared Ta_2O_5 nanoparticles when dispersed in methanol (left) and etched with hydrochloric acid for 25 min. After centrifugation, the hydroxyl-terminated nanoparticles were transferred into an acrylic acid solution (center) and heated up to 80 ± 1 °C for different polymerization times.

In general, pristine Ta_2O_5 and Ta_2O_5-PAA NPs are mostly spherical and ellipsoidal in shape and tend to form agglomerates with > 100 nm in size, which is observed for both Ta_2O_5 and Ta_2O_5-PAA and is probably due to their high surface energy [32]. The single particle size of the uncoated Ta_2O_5 NPs varies between 13 – 57 nm with an average particle size of 26.6 ± 5.9 nm (Figure 1b). These findings agree with the mean crystallite size calculated via the Scherrer equation and indicate that the Ta_2O_5 NPs are an excellent candidate for the design of theranostic systems since it has been shown that a particle size of up to 50 nm results in high cellular uptake [33].

The TEM images of the Ta_2O_5-PAA nanocomposites show homogeneous coverage of the surfaces of individual Ta_2O_5 NPs with layers of PAA. It is also demonstrated that the PAA layer thickness increases with increasing polymerization time: while polymerization for 1 h yields a polymer thickness of 2.1 ± 0.7 nm, a polymerization time of 2.5 and 5 h leads to a thickness of 3.9 ± 0.9 nm and 8.2 ± 1.4 nm, respectively.

The polymerization of the acrylic acid (AA) around individual particles is only possible if the surface Ta_2O_5 NPs are activated to induce preferential polymerization sites for the AA monomer, ensuring that the polymer chains grow around each individual ceramic particle, avoiding cluster formation Ta_2O_5 (Figures 1c and 1f) [34, 35]. Layer thickness is associated with the amount of drug that can be uptake and influences its release properties.

Chemical and thermal properties of the Ta_2O_5 NPs and Ta_2O_5-PAA NPs: The FTIR spectrum of uncoated Ta_2O_5 NPs with presents bands at around 880 and 680 cm^{-1} assigned to the Ta-O-Ta bridge and stretching vibrations of Ta-O bonds (Figure 2a), respectively [36].

The FTIR spectra of the Ta_2O_5-PAA nanocomposites show the presence of Ta-O and Ta-O-Ta vibrations in low wavenumbers < 900 cm^{-1}, which overlap with the polymer stretching and bending vibrations. The characteristic O-H out-of-plane bending, and CH_2 and C-COOH stretching are observed at 914 and 797 cm^{-1}, respectively [37]. Besides these bands, all other characteristic absorption bands that correspond to PAA are present in the Ta_2O_5-PAA nanocomposites: the absorption bands at 2946, 1451, and 1108 cm^{-1} correspond to CH_2 or CH stretching, CH_2 stretching, and C-CH_2 stretching, respectively [37, 38]. In addition, the absorption bands at 1704 and 1240 cm^{-1} are ascribed to the C-O stretching and C=O stretching, respectively [37]. It was interesting to observe that the vibration band with a maximum at 1704 cm^{-1} increased with the polymerization time.

The monomer AA typically shows absorption bands at 1600 – 1680 cm^{-1}, which are assigned to C=C stretching [39]. The absence of these absorption bands in the FTIR spectra of the Ta_2O_5-PAA nanocomposites suggests the presence of polymer chains around the Ta_2O_5 nanoparticles. The increase in polymerization time generally leads to an increase in the intensity of the

absorption bands of the PAA characteristic functional groups, without changing their wavenumber.

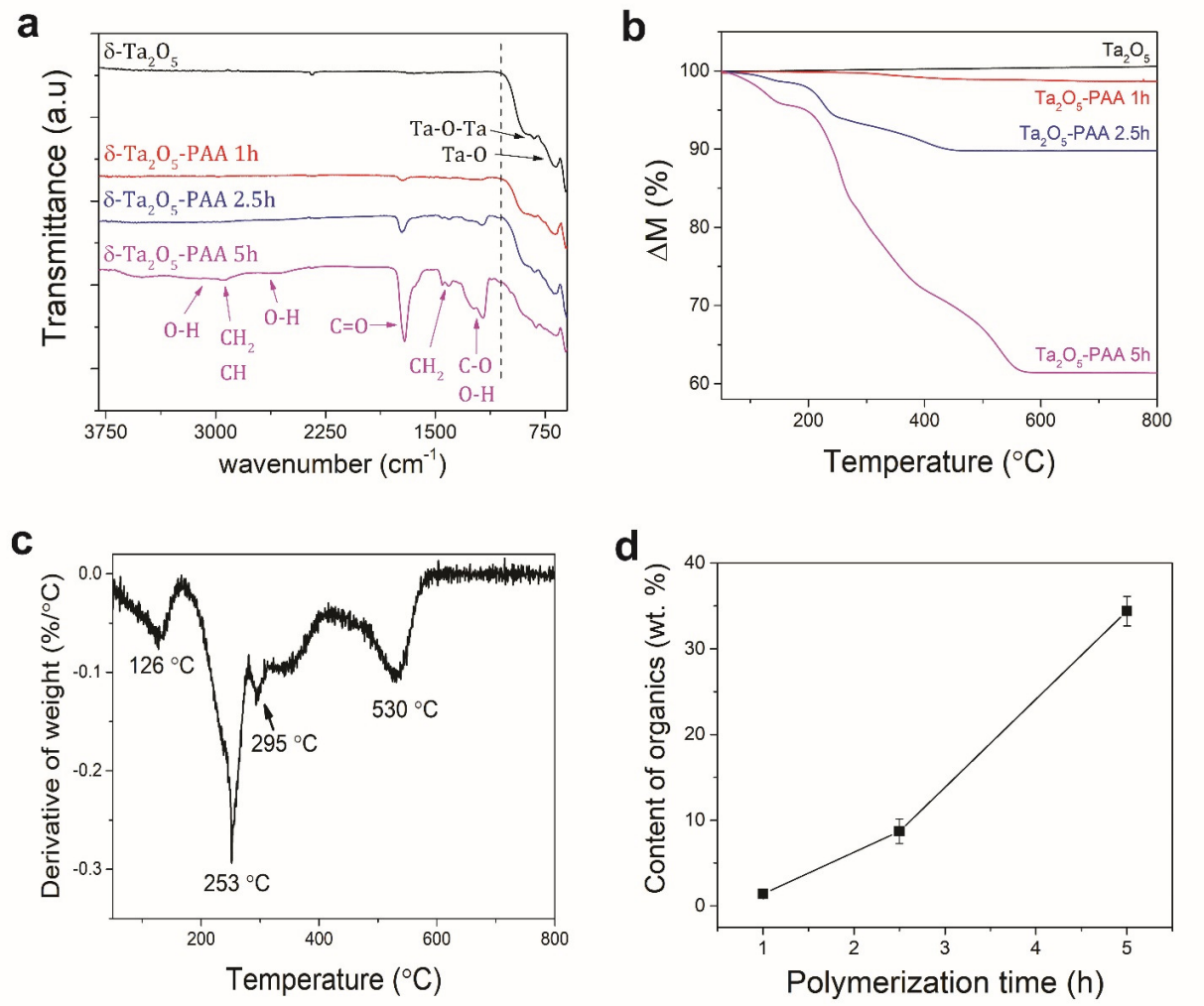

Figure 2. a) FTIR spectra of Ta_2O_5 NPs and Ta_2O_5-PAA nanocomposites with a polymerization time of 1, 2.5, and 5 h. The dotted line indicates the wavenumber, below which the absorption bands of Ta_2O_5 outweigh the absorption bands related to PAA, b) TGA curves of Ta_2O_5 NPs and Ta_2O_5-PAA nanocomposites with a polymerization time of 1, 2.5, and 5 h, c) First derivative of the TGA curve of Ta_2O_5-PAA with 5 h polymerization time, and d) Plot of the content of the organics as a function of the polymerization time.

Uncoated Ta_2O_5 NPs did not show any mass loss for the entire temperature scan range, while the Ta_2O_5-PAA nanocomposite materials exhibited characteristic mass losses that were due to the presence of the polymer on their surfaces (Figure 2b). Furthermore, a mass loss starting at 126 °C can be observed for all polymer nanocomposite materials and corresponds to the loss of unbound water, related to absorbed moisture present in the polymer nanolayer and is due to storage under ambient conditions (Figure 2c). The amount of water was determined to be 0.1, 1.4, and 4.3 wt.% for the Ta_2O_5-PAA nanocomposite with a polymerization time of 1, 2.5, and 5 h, respectively.

For all the PAA-containing materials, three additional mass losses were identified at 253, 295, and 530 °C, which is related to the release of organic compounds. The second mass loss can be attributed to the formation of PAA anhydride, and the third one corresponds to the degradation of the PAA anhydride [40]. The final thermal decomposition of the polymer occurs at a temperature above 500 °C [40].

The amount of polymer that wraps individual Ta_2O_5 nanoparticles increases with polymerization time, reaching a maximum of 34 wt.% for the nanocomposite sample polymerized during 5 h and is in accordance with the increase of the polymer layer thickness, previously observed in figure 1.

Surface Composition of the Nanomaterials before and after Polymerization: The surface composition of the prepared Ta_2O_5 NPs was evaluated via X-ray photoelectron spectroscopy (XPS) and compared to Ta_2O_5 after additional treatment with HCl to show that the latter sample shows surface functionalization with hydroxyl groups, which, in turn, facilitate the polymerization of AA onto the NP surfaces.

High-resolution XPS survey spectra show typical peaks that can be ascribed to the presence of carbon, oxygen, and tantalum (Figure 3, and all XPS data are summarized in Tables S1 and S2 of the Supporting Information). The peaks at a lower binding energy of ~285 and ~286 eV can be assigned to CH_2 and CH, respectively [41]. The peak at ~288 eV is ascribed to C–O bonds, which indicates the presence of adventitious carbon. The nanocomposites display an additional peak at ~290 eV, which corresponds to the O–C=O groups that are found in PAA [41]. Table 1 displays the C 1s envelope ratios for all samples and shows, besides the increase in the C/O ratio, from ~143% (Ta_2O_5) to ~218% (Ta_2O_5-PAA), an increase in the amount of CH bonds that are typically found in the polymer chains, underlining the successful polymerization of PAA onto the NPs surface. These findings are further supported by the presence of an O 1s peak at ~534 eV for the O–C=O group, which is only found in the Ta_2O_5-PAA nanocomposites [41].

The O 1s spectra also display peaks that correspond to Ta–O bonds and –OH groups at a binding energy of ~531 and 533 eV, respectively [42]. The presence of hydroxyl groups on the surface of Ta_2O_5 after treatment with HCl is of importance, since the –OH groups act as activation sites that react with the AA monomers on the NP surfaces to form a layer of PAA, as shown via TEM (Figures 1e and 1f). Furthermore, the O 1s envelope ratios are shown in Table S3

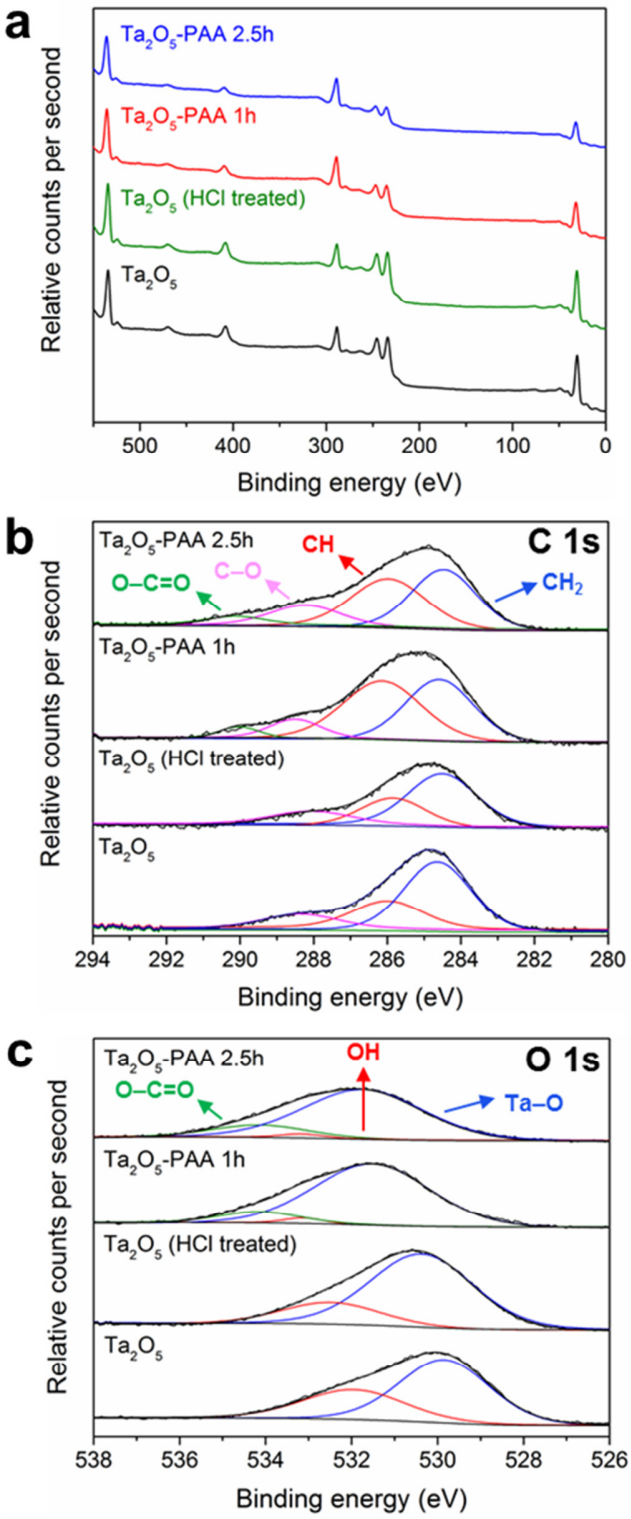
a
Ta2O5-PAA 2.5h
Ta2O5-PAA 1h
Ta2O5 (HCl treated)
Ta2O5
Relative counts per second
500
400
300
200
100
0
Binding energy (eV)
b
Ta2O5-PAA 2.5h
CH
C 1s
O–C=O
C–O
CH2
Ta2O5-PAA 1h
Ta2O5 (HCl treated)
Ta2O5
Relative counts per second
294
292
290
288
286
284
282
280
Binding energy (eV)
c
Ta2O5-PAA 2.5h
OH
O 1s
O–C=O
Ta–O
Ta2O5-PAA 1h
Ta2O5 (HCl treated)
Ta2O5
Relative counts per second
538
536
534
532
530
528
526
Binding energy (eV)

Figure 3. a) XPS survey spectra of Ta_2O_5 NPs, Ta_2O_5 NPs after HCl treatment, Ta_2O_5-PAA 1 h, and Ta_2O_5-PAA 2.5 h. High-resolution spectra of Ta_2O_5 NPs and Ta_2O_5 NPs after HCl treatment and Ta_2O_5-PAA nanocomposites with polymerization times of 1 and 2.5 h for b) the C 1s region and c) the O 1s region. The spectra have been corrected to C–C at 284.8 eV.

Table 1. XPS analysis including the C 1s region of Ta_2O_5 NPs (before and after treatment with HCl) and Ta_2O_5-PAA composite nanoparticles.

Sample	**XPS C 1s envelope ratios (%)**				**C/O ratio (%)**
	CH_2	**CH**	**C–O**	**O–C=O**	
Ta_2O_5	61.05	25.24	13.71	–	145.38
Ta_2O_5 (HCl treated)	55.87	28.51	15.62	–	140.92
Ta_2O_5-PAA 1 h	41.70	44.81	9.13	4.36	216.94
Ta_2O_5-PAA 2.5 h	40.39	40.40	13.81	5.40	218.17

In Vitro CT Imaging of Ta_2O_5-PAA Nanocomposites: The anatomical contrast enhancement capability of uncoated Ta_2O_5 NPs and the Ta_2O_5-PAA nanocomposite with high polymerization time (5 h) was demonstrated using a clinical CT scanner, with the resulting CT number as a function of the tantalum concentration, as shown in Figure 4. The results of the CT scans of uncoated Ta_2O_5 NPs are shown in Figure S1.

The CT values in Hounsfield Units (HU) for each concentration were determined for multiple regions along the central axis of the vial to account for possible sedimentation of the suspended nanoparticles (see red dashed lines on Figure 4).

In general, the contrast increased with increasing concentration of tantalum, and the suspension remained stable up to a concentration of 8 mg/mL for the Ta_2O_5-PAA nanocomposite. For the uncoated Ta_2O_5 NPs, however, a noticeable difference in CT number was observed at the highest concentration of 8 mg/mL for the center of the composite sediment and the center of the suspension height, which ultimately underlines the stabilization effect of PAA on the suspension. The data were plotted and fitted to deduce the relationship between the CT number and the tantalum concentration. The average CT number was chosen across the suspension height. It should be noted that the CT number reached a value of 1000 – 2000 HU in the sediment at a tantalum concentration of 8 mg/mL for uncoated Ta_2O_5, which highlights the potential of Ta_2O_5 as an anatomical contrast enhancement agent. These results agree with reported CT numbers for Ta-containing compounds and underline the improved suspension stability and reduced beam hardening in comparison to previously reported Bi_2O_3 nanoparticles [3, 43].

The PAA layer on the surface of the ceramic particles increased the nanocomposite stability in the liquid media, preventing deposition and agglomeration, leading to a superior contrast enhancement and contrast-to-noise ratio of Ta_2O_5-PAA for high X-ray energies are of particular interest in a clinical setup [44]. Although it is beneficial for pediatric patients to reduce the radiation dose, the ability to use high X-ray energies is important for the imaging of large patients, as enough penetration of X-rays needs to be ensured to obtain images of the desired quality.

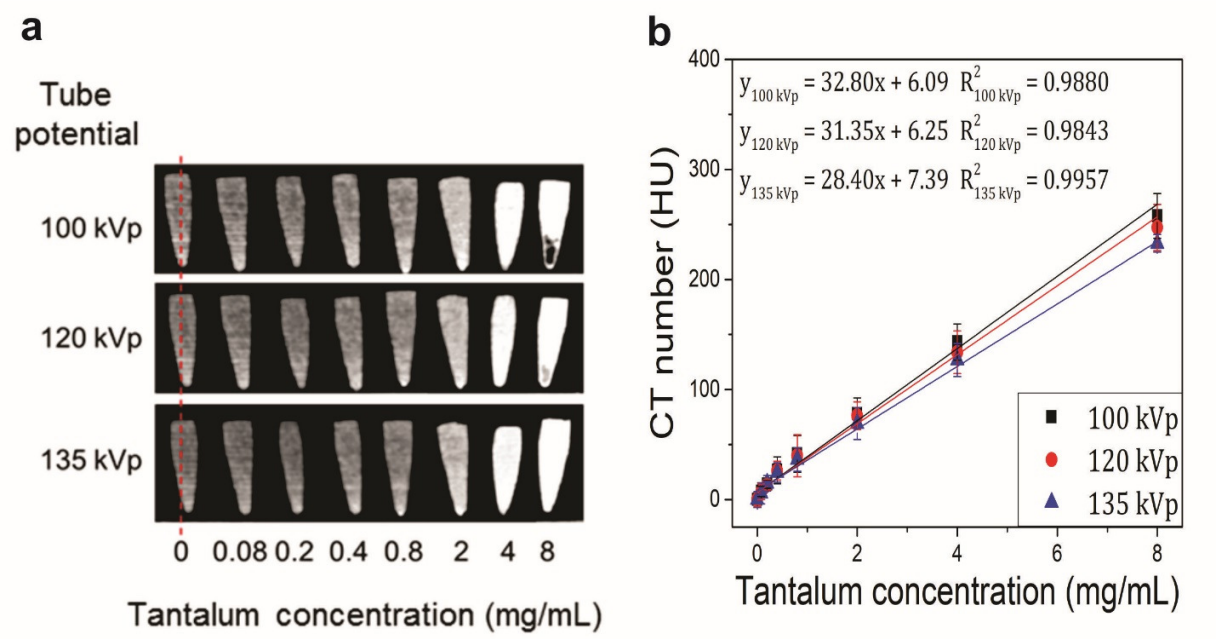

Figure 4. a) CT images of Ta_2O_5-PAA NPs (5h polymerization) with Ta mass concentrations of 0 – 8 mg/mL; the red dashed line indicates the area which was used to determine the CT number (suspension height and sediment). The tube potential varied between 100, 120, and 135 kVp and b) Linear fitting of the CT number of Ta_2O_5-PAA NPs (5h polymerization) as a function of the mass concentration of Ta in mg/mL at different tube potentials of 100, 120, and 135 kVp. The equation of the linear regression and the R^2 value are indicated.

Swelling and MTX Capacity of Ta_2O_5-PAA Nanocomposites: Investigation of the swelling behavior of PAA-containing nanomaterials is of importance since the swelling property influences the diffusion of small molecules through the polymer matrix. PAA is a hydrogel and increasing its content leads to larger water affinity, which ultimately results in higher swelling ratios (SR) [45].

The swelling kinetics of the Ta_2O_5 NPs and the Ta_2O_5-PAA nanocomposites for a time frame of 0 – 48 h at 37 °C and pH 7.4 are displayed in Figure 5a. As the thickness of the PAA layer

increases, the volume of the hydrogel also increases, and consequently the swelling ratio. In general, the swelling ratio increases rapidly in the first 4 h and reaches equilibrium after around 24 h.

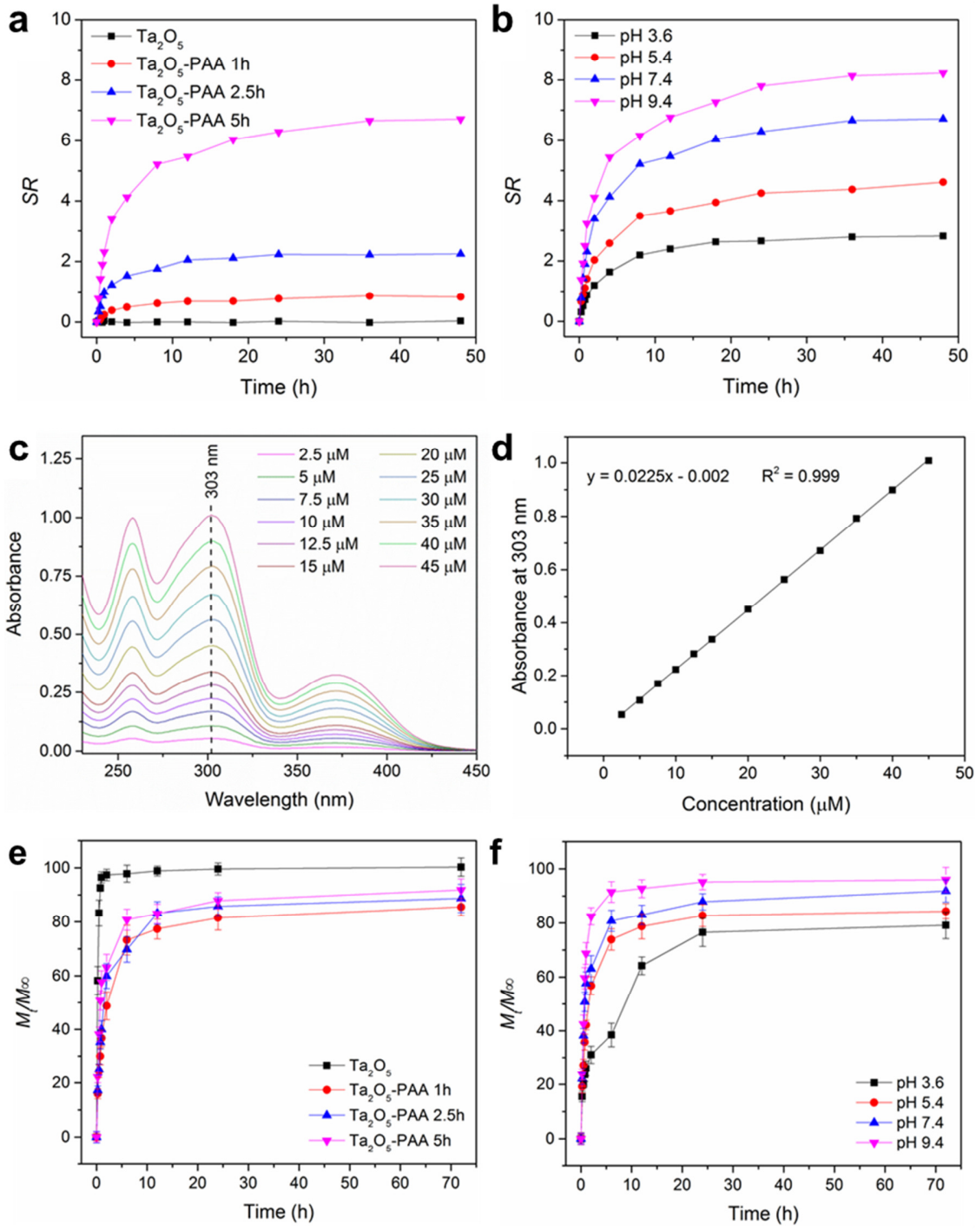

Figure 5. a) Swelling ratio of Ta_2O_5 NPs and Ta_2O_5-PAA nanocomposites with polymerization times of 1, 2.5, and 5 h. The swelling properties were measured at 37 ºC, at pH 7.4 for 48 h, b) The influence of the pH value of the buffer solution on the swelling ratio of the Ta_2O_5-PAA nanocomposite that was synthesized with a polymerization time of 5 h. The swelling properties were measured at 37 ºC, at pH 3.6, 5.4, 7.4, and 9.4 for 48 h, c) The absorbance of MTX solution at concentrations ranging from 2.5 – 45 µM, d) Calibration curve and the equation for the calculation of MTX concentration. *In vitro* release profiles of e) MTX-soaked Ta_2O_5 NPs and Ta_2O_5-PAA nanocomposites with different polymerization times of 1, 2.5, and 5 h in a buffer solution with pH 7.4, and f) Ta_2O_5-PAA with longest polymerization time of 5 h in buffer solutions with pH values of 3.6, 5.4, 7.4, and 9.4. The drug release was monitored at 37 ºC for 72 h.

To study the effect of pH on the swelling ratio, we chose the nanocomposite with the highest amount of PAA (Ta_2O_5-PAA 5 h) and exposed it to buffer solutions with different pH (pH 3.6, 5.4, 7.4, and 9.4) at 37 ºC (Figure 5b).

The difference in swelling ratio is ascribed to the accessibility of free volume for the expanded polymer matrix, the polymer chain relaxation, and the availability of ionizable functional groups [45]. For instance, the presence of carboxyl groups can lead to the formation of hydrogen bonds with water. In addition, the swelling behavior depends on the network swelling pressure, the dissociation equilibrium and the presence of ions and impurities in the swelling medium [46].

The carboxylic acid group in PAA tends to dissociate at pH values greater than 4.5, which ultimately leads to an increase in osmotic pressure inside the polymer matrix and explains the low swelling ratio in the buffer solution of pH 3.6 [45]. With increasing pH, the dissociation of

carboxylic groups increases, which leads to negatively charged polymer chains that repel each other[45], creating more free space between the polymer chains, ultimately leading to an increase in the swelling ratio.

When the hydrogel is placed into the aqueous solution containing MTX, the polymer network starts to swell, and the drug molecules will penetrate and fill the space between the polymer chains. The thicker the polymer layer, the larger is the swelling ratio (Figure 5a). The MTX molecules and PAA chains experience electrostatic repulsion at a pH of 7.4, which could explain the low increase in loading capacity for the nanocomposite with thickest polymer layer [29, 31, 47]. The effects are described in more detail in the next section (Figure 6).

The MTX entrapment per 1 mg of the nanocomposite was also determined via UV-vis spectroscopy after the *in vitro* drug release experiments and the treatment of the composites with 0.1 M NaOH. The calibration curve of different concentrations of MTX was determined and is shown in Figures 5c and 5d. The MTX entrapment obtained via UV-vis spectroscopy corroborates the value calculated through the dry weight of the composite after the drug loading (Table 2).

Table 2. Loading capacity (LC) and entrapment efficiency (EE) of Ta_2O_5 NPs and Ta_2O_5-PAA composite nanoparticles with different polymerization times at a weight ratio of MTX/composite of 1/1 (10 mg/mL).

Sample	**MTX/ 1 mg composite (dry weight) [µg]**	**MTX LC and EE [%][a]**	**MTX LC and EE [%][b]**	**MTX/ 1 mg composite (UV-vis) [µg]**
Ta_2O_5	11.5 ± 0.7	1.2 ± 0.1	-	8.3 ± 1.31
Ta_2O_5-PAA 1 h	21.3 ± 2.5	2.1 ± 0.3	95.5 ± 11.2	20.2 + 2.9
Ta_2O_5-PAA 2.5 h	76.6 ± 9.3	7.7 ± 0.9	75.7 ± 9.2	67.5 ± 5.6
Ta_2O_5-PAA 5 h	126.4 ± 8.7	12.6 ± 0.9	31.6 ± 2.2	118.0 ± 4.1

[a] Normalized to the mass of composite.

[b] Normalized to the mass of PAA.

The reported drug loading capacities for similar systems range from 12 – 80%, based on the delivery system components, the drug entrapment method, the incubation time, and the drug concentration used for the entrapment [29, 31, 48, 49]. For instance, it was shown for DOX as a model drug and a system consisting of mesoporous silica and PAA, that by increasing the weight ratio of drug/hydrogel from 0.1 to 1.0, the loading capacity increased from 2.2 to 40.2% [30], and with an entrapment efficiency that ranges from 25.1 to 80.4%, respectively [30].

Ta_2O_5-PAA nanocomposites showed an entrapment efficiency up to 95% for the sample with the thin PAA layer, down to 32% for the sample with 8.2 ± 1.4 nm polymer layer surrounding the ceramic particle (table 2).

Effect of PAA Layer Thickness on the Release of MTX from Ta_2O_5-PAA Nanocomposites: Drug release kinetics, measured at different pHs's and for the samples with different polymer shell thickness was studied according to the mathematical model developed by Ritger-Peppas:

$$\frac{M_t}{M_\infty} = kt^n \qquad (6)$$

where M_∞ is the total amount of drug, M_t is the amount of drug released at time t, k is a kinetic constant, and n is the diffusion exponent. For modeling, only fractions < 0.6 were considered.

It was observed that for all tested samples, a burst release of MTX occurred in the first hour, which is due to desorption of MTX from the gel surface. The following release of the drug was slower and after 72 h, it yielded a total release of MTX of 100% for the Ta_2O_5 NPs, and 86, 89, and 92% for the Ta_2O_5-PAA nanocomposites with a polymerization time of 1, 2, and 5 h, respectively. The fast release of MTX from the uncoated Ta_2O_5 NPs is related to the absence of a protective hydrogel shell that creates a physical barrier, delaying the release.

When the MTX-loaded hydrogel is placed in the release medium, the polymer starts to swell, followed by polymer chain relaxation and volume expansion. This enables the trapped MTX to diffuse into the external release medium [47]. The observed release rate tends to increase with increasing polymer layer thickness, which is directly connected to the increase in drug loading (Figure 5e).

The drug release kinetics of Ta_2O_5 NPs was impossible to determine due to the boost of drug release to the buffer solution that started immediately after immersion of the particles in the media. A value for *n* between 0.54 and 0.71 was obtained for all the nanocomposites and indicates that the drug transport mechanism appears to be anomalous: the drug release is controlled by a coupled effect of Fickian diffusion and chain relaxation of the hydrogels (Table 3).

Table 3. Ritger-Peppas fitting parameters obtained for Ta_2O_5-PAA composite nanoparticles with different polymerization times.

Sample	***k***	***n***	**R^2**	**Transport mechanism**
Ta_2O_5-PAA 1 h	1.54 ± 0.01	0.54 ± 0.03	0.990	Diffusion and relaxation controlled
Ta_2O_5-PAA 2.5 h	1.60 ± 0.01	0.61 ± 0.03	0.992	Diffusion and relaxation controlled
Ta_2O_5-PAA 5 h	1.78 ± 0.02	0.71 ± 0.05	0.987	Diffusion and relaxation controlled

Effect of pH on the Drug Release Kinetics: To evaluate the effects of pH on the overall drug release and its mechanism, the Ta_2O_5-PAA (5 h polymerization time) soaked with MTX was placed in the release buffers with pH of 3.6, 5.4, 7.4, and 9.4 (Figure 5f). The drug release from the nanocomposites follows a similar profile for all tested pH values, starting with the initial burst release of MTX, which is followed by the slow release at longer incubation times. While the total release of MTX is only 79% at a pH of 3.6, the drug release increases to 84, 92, and

96% for pH of 5.4, 7.4, and 9.4, respectively. Moreover, the initial burst release of MTX was significantly reduced for the lowest pH of 3.6, showing that the swelling of the PAA nanolayer is the principal parameter ruling drug release (Figure 5b). Since the swelling ratio increases with increasing pH of the buffer solution and entraps more drug into the polymer network, and consequently more drug can be released from the hydrogel as the structure becomes more open [47].

The analysis of the drug release kinetics indicates that the release mechanism strongly depends on the pH of the release medium [27, 45, 47]. The diffusion exponent n increased as the pH of the release medium became more alkaline, which underlines the pH sensitivity of PAA-containing hydrogels (Table 4). For a pH of 3.6, the release followed Fickian diffusion ($n < 0.5$). With regard to the release of MTX, Fick's law includes the adsorption of buffer on the polymer matrix and the simultaneous desorption of MTX via diffusion [27]. For pH values of 5.4 and 7.4, the increase in the diffusion coefficient ($n = 0.54 \pm 0.03$ to 0.71 ± 0.05) suggesting that the release mechanism is a result of the contributions of both Fickian diffusion and relaxation of polymer chains. At a pH of 9.4, the extensive ionization of the functional groups significantly influences the polymer chain relaxation and consequently, leads to a transport mechanism that is closer to Case II transport ($n = 0.84 \pm 0.01$).

Table 4. Ritger-Peppas fitting parameters obtained for theTa_2O_5-PAA composite nanoparticles with 5 h polymerization time, exposed to different pH environments.

Sample	*k*	*n*	R^2	Transport mechanism
pH 3.6	1.39 ± 0.01	0.28 ± 0.03	0.966	Diffusion controlled
pH 5.4	1.61 ± 0.01	0.54 ± 0.03	0.992	Diffusion and relaxation controlled
pH 7.4	1.78 ± 0.02	0.71 ± 0.05	0.987	Diffusion and relaxation controlled
pH 9.4	1.88 ± 0.01	0.84 ± 0.01	0.999	Relaxation controlled

In addition to the effect of the swelling ratio, the presence of electrostatic interactions between the drug and the hydrogel can also influence the drug release [29, 31, 47], as schematically shown in Figure 6. MTX has three pK_a values at 3.8, 4.8, and 5.6, while the dissociation of the carboxylic group of PAA takes place at pK_a of 4.25 [50]. At pH 3.6, the nitrogen atom in the pteridine ring should be mainly protonated, while the carboxylic groups on the hydrogel are hardly ionized. This leads to the presence of weak hydrogen bonding between the carboxylic groups of MTX and PAA. At pH 5.4, the carboxylic groups on the PAA chains are partly deprotonated and form carboxylate anions, which leads to fewer hydrogen bonds. Moreover, the carboxylic groups of the MTX molecule start to dissociate, which causes further negative charge and consequently, increases the electrostatic repulsion between the MTX molecule and the PAA chains.

At pH of 7.4 and 9.4, the nitrogen atom of the pteridine ring is mostly deprotonated, which further increases the electrostatic repulsion between the MTX molecule and the PAA. The increase in pH shifts the equilibrium further to dissociated components and increases the

electrostatic repulsion and the release of MTX. Moreover, the solubility of PAA increases with increasing pH, which can lead to the degradation and erosion of the polymer matrix and thus, to the increased release of entrapped MTX, especially for long incubation times [51, 52].

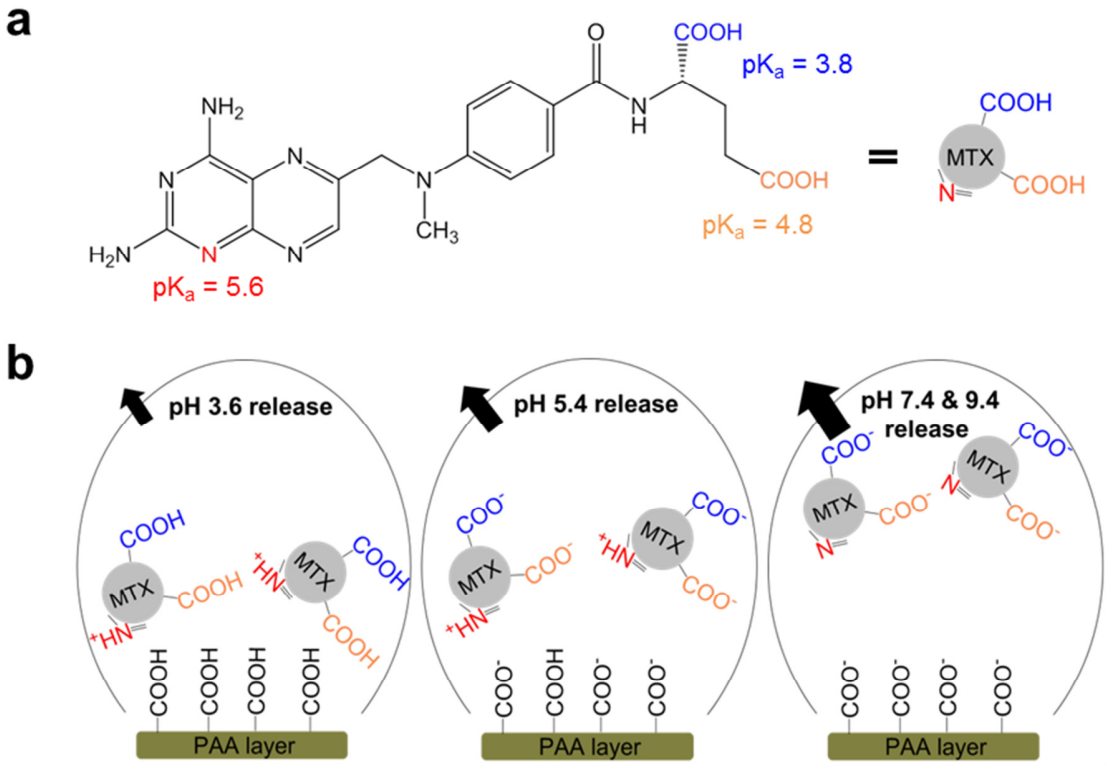

Figure 6. a) Structure of MTX, and b) Schematic route of the MTX loading and release from the nanocomposites containing PAA at different pH values (3.6, 5.4, 7.4, and 9.4).

CONCLUSIONS

To design a theranostic system with controlled drug release properties, Ta_2O_5-PAA nanocomposites were prepared through the polymerization of AA on the surfaces of individual Ta_2O_5 NPs. By varying the polymerization time, different layer thicknesses of PAA on the surfaces of the ceramic particles were obtained, which ultimately had an impact on the drug loading capacity.

MTX-loaded Ta_2O_5-PAA matrices were prepared by soaking Ta_2O_5-PAA in a solution of MTX, and the release mechanism was studied by the Ritger-Peppas model. It was demonstrated that the Ta_2O_5-PAA nanocomposites were highly sensitive to different pH environments. Firstly, the swelling ratio increased with increasing pH of the swelling medium. Secondly, an acidic release medium slowed down the release of MTX, while more alkaline pH values led to a quick release of MTX from the MTX-loaded Ta_2O_5-PAA matrices. The diffusion exponent *n* increased from 0.28 to 0.84, which suggests that, with increasing pH, polymer chain relaxation contributes to the transport mechanism. These results indicate that such a system may, under certain conditions, provide release characteristics approaching zero-order release.

Furthermore, the Ta_2O_5-PAA nanocomposites showed a contrast enhancement for tube potentials ranging from 100 – 135 kVp *in vitro*. The image consistency at high X-ray energies is of interest in a clinical setup, as it ensures enough penetration of X-rays in larger patients.

The results evidence that Ta_2O_5-PAA nanocomposites can be successfully used as drug delivery systems, providing imaging, therapeutic, targeting, and potentially, radiation dose enhancement functionalities on one single platform.

ACKNOWLEDGMENTS

This work was supported by the Australian Research Council (ARC DP160102627) and the National Health and Medical Research Council (APP1084994). Furthermore, the authors acknowledge the use of the facilities within the Electron Microscopy Centre at the University of Wollongong and the assistance of Dr. D. Cardillo in acquiring the TEM images. We would also like to thank Dr. T. Silver for help with editing the manuscript and Dr. D. Shi at the University of Wollongong for conducting the XPS measurements.

REFERENCES

[1] N.C. Institute, 2017. http://www.cancer.gov/cancertopics/factsheet/Therapy/radiation.

[2] C. Cheng, A. Amini, C. Zhu, Z. Xu, H. Song, N. Wang, Enhanced photocatalytic performance of TiO2-ZnO hybrid nanostructures, Scientific reports 4 (2014) 4181.

[3] K. Bogusz, M. Tehei, C. Stewart, M. McDonald, D. Cardillo, M. Lerch, S. Corde, A. Rosenfeld, H.K. Liu, K. Konstantinov, Synthesis of Potential Theranostic System Consisting of Methotrexate-Immobilized (3-Aminopropyl) Trimethoxysilane Coated α-Bi_2O_3 Nanoparticles for Cancer Treatment, RSC Adv. 4(46) (2014) 24412-24419.

[4] H. Maeda, J. Wu, T. Sawa, Y. Matsumura, K. Hori, Tumor vascular permeability and the EPR effect in macromolecular therapeutics: a review, Journal of controlled release 65(1) (2000) 271-284.

[5] R. Brown, M. Tehei, S. Oktaria, A. Briggs, C. Stewart, K. Konstantinov, A. Rosenfeld, S. Corde, M. Lerch, High□Z Nanostructured Ceramics in Radiotherapy: First Evidence of Ta2O5□ Induced Dose Enhancement on Radioresistant Cancer Cells in an MV Photon Field, Particle & Particle Systems Characterization 31(4) (2014) 500-505.

[6] P.J. Bonitatibus Jr, A.S. Torres, G.D. Goddard, P.F. FitzGerald, A.M. Kulkarni, Synthesis, characterization, and computed tomography imaging of a tantalum oxide nanoparticle imaging agent, Chemical Communications 46(47) (2010) 8956-8958.

[7] W. Yang, Y. Liu, Q. Zhang, Y. Leng, H. Zhou, P. Yang, J. Chen, N. Huang, Biomedical response of tantalum oxide films deposited by DC reactive unbalanced magnetron sputtering, Surface and Coatings Technology 201(19) (2007) 8062-8065.

[8] B.F. Mullan, M.T. Madsen, L. Messerle, V. Kolesnichenko, J. Kruger, X-ray attenuation coefficients of high-atomic-number, hexanuclear transition metal cluster compounds: A new paradigm for radiographic contrast agents, Academic radiology 7(4) (2000) 254-259.

[9] S.-H. Lee, J. Kim, S.-J. Kim, S. Kim, G.-S. Park, Hidden structural order in orthorhombic Ta 2 O 5, Physical review letters 110(23) (2013) 235502.

[10] S. Pérez-Walton, C. Valencia-Balvín, A. Padilha, G. Dalpian, J. Osorio-Guillén, A search for the ground state structure and the phase stability of tantalum pentoxide, Journal of Physics: Condensed Matter 28(3) (2015) 035801.

[11] J. Nadel, W. Dodds, H. Goldberg, P. Graf, Insufflation of Powdered Tantalum in the Esophagus: New Esophagographic Technique, Investigative radiology 4(2) (1969) 57-62.

[12] A. Jakhmola, N. Anton, T.F. Vandamme, Inorganic nanoparticles based contrast agents for X□ray computed tomography, Advanced healthcare materials 1(4) (2012) 413-431.

[13] S.M. Janib, A.S. Moses, J.A. MacKay, Imaging and drug delivery using theranostic nanoparticles, Advanced drug delivery reviews 62(11) (2010) 1052-1063.

[14] O. Rabin, J.M. Perez, J. Grimm, G. Wojtkiewicz, R. Weissleder, An X-ray computed tomography imaging agent based on long-circulating bismuth sulphide nanoparticles, Nature materials 5(2) (2006) 118-122.

[15] T.M. Allen, P.R. Cullis, Drug delivery systems: entering the mainstream, Science 303(5665) (2004) 1818-1822.

[16] Y.-E.L. Koo, G.R. Reddy, M. Bhojani, R. Schneider, M.A. Philbert, A. Rehemtulla, B.D. Ross, R. Kopelman, Brain cancer diagnosis and therapy with nanoplatforms, Advanced drug delivery reviews 58(14) (2006) 1556-1577.

[17] D.F. Emerich, C.G. Thanos, The pinpoint promise of nanoparticle-based drug delivery and molecular diagnosis, Biomolecular engineering 23(4) (2006) 171-184.

[18] K.E. Uhrich, S.M. Cannizzaro, R.S. Langer, K.M. Shakesheff, Polymeric systems for controlled drug release, Chemical reviews 99(11) (1999) 3181-3198.

[19] E. Caló, V.V. Khutoryanskiy, Biomedical applications of hydrogels: A review of patents and commercial products, European Polymer Journal 65 (2015) 252-267.

[20] A. Usta, Synthesis, analysis, and characterization of electrically sensitive PVA hydrogels loaded with MTX cancer drugs, Wichita State University, 2014.

[21] W. Cheng, C. Liang, L. Xu, G. Liu, N. Gao, W. Tao, L. Luo, Y. Zuo, X. Wang, X. Zhang, X. Zeng, L. Mei, TPGS-Functionalized Polydopamine-Modified Mesoporous Silica as Drug Nanocarriers for Enhanced Lung Cancer Chemotherapy against Multidrug Resistance, Small 13(29) (2017) 1700623.

[22] W. Cheng, J. Nie, N. Gao, G. Liu, W. Tao, X. Xiao, L. Jiang, Z. Liu, X. Zeng, L. Mei, A Multifunctional Nanoplatform against Multidrug Resistant Cancer: Merging the Best of Targeted Chemo/Gene/Photothermal Therapy, Advanced Functional Materials 27(45) (2017) 1704135.

[23] Drugs.com, 2017. http://www.drugs.com/sfx/methotrexate-side-effects.html.

[24] N. Kohler, C. Sun, J. Wang, M. Zhang, Methotrexate-modified superparamagnetic nanoparticles and their intracellular uptake into human cancer cells, Langmuir 21(19) (2005) 8858-8864.

[25] B.A. Chabner, D.L. Longo, Cancer Chemotherapy and Biotherapy: Principles and Practice, Wolters Kluwer Health/Lippincott Williams & Wilkins2010.

[26] S. Ray, M. Joy, B. Sa, S. Ghosh, J. Chakraborty, pH dependent chemical stability and release of methotrexate from a novel nanoceramic carrier, RSC Advances 5(49) (2015) 39482-39494.

[27] S.W. Kim, Y.H. Bae, T. Okano, Hydrogels: swelling, drug loading, and release, Pharmaceutical research 9(3) (1992) 283-290.

[28] L.-G. Chen, Z.-L. Liu, R.-X. Zhuo, Synthesis and properties of degradable hydrogels of konjac glucomannan grafted acrylic acid for colon-specific drug delivery, Polymer 46(16) (2005) 6274-6281.

[29] Y. Dai, C. Zhang, Z. Cheng, P.a. Ma, C. Li, X. Kang, D. Yang, J. Lin, pH-responsive drug delivery system based on luminescent CaF 2: Ce 3+/Tb 3+-poly (acrylic acid) hybrid microspheres, Biomaterials 33(8) (2012) 2583-2592.

[30] H. Li, J.Z. Zhang, Q. Tang, M. Du, J. Hu, D. Yang, Reduction-responsive drug delivery based on mesoporous silica nanoparticle core with crosslinked poly (acrylic acid) shell, Materials Science and Engineering: C 33(6) (2013) 3426-3431.

[31] S. Rasouli, S. Davaran, F. Rasouli, M. Mahkam, R. Salehi, Synthesis, characterization and pH-controllable methotrexate release from biocompatible polymer/silica nanocomposite for anticancer drug delivery, Drug delivery 21(3) (2014) 155-163.

[32] H.C. Huang, T.E. Hsieh, Preparation and characterizations of tantalum pentoxide (Ta2O5) nanoparticles and UV□curable Ta2O5□acrylic nanocomposites, Journal of Applied Polymer Science 117(3) (2010) 1252-1259.

[33] A. Malugin, H. Ghandehari, Cellular uptake and toxicity of gold nanoparticles in prostate cancer cells: a comparative study of rods and spheres, Journal of Applied Toxicology 30(3) (2010) 212-217.

[34] J. Jordan, K.I. Jacob, R. Tannenbaum, M.A. Sharaf, I. Jasiuk, Experimental trends in polymer nanocomposites—a review, Materials Science and Engineering: A 393(1) (2005) 1-11.

[35] K. Müller, E. Bugnicourt, M. Latorre, M. Jorda, Y. Echegoyen Sanz, J. Lagaron, O. Miesbauer, A. Bianchin, S. Hankin, U. Bölz, G. Pérez, M. Jesdinszki, M. Lindner, Z. Scheuerer, S. Castelló, M. Schmid, Review on the Processing and Properties of Polymer Nanocomposites and Nanocoatings and Their Applications in the Packaging, Automotive and Solar Energy Fields, Nanomaterials 7(4) (2017) 74.

[36] Y. Shin, J.Y. Kim, C. Wang, J.F. Bonnet, K.S. Weil, Controlled deposition of covalently bonded tantalum oxide on carbon supports by solvent evaporation sol–gel process, Surface Science 603(15) (2009) 2290-2293.

[37] J. Dong, Y. Ozaki, K. Nakashima, Infrared, Raman, and near-infrared spectroscopic evidence for the coexistence of various hydrogen-bond forms in poly (acrylic acid), Macromolecules 30(4) (1997) 1111-1117.

[38] L.J. Kirwan, P.D. Fawell, W. van Bronswijk, In situ FTIR-ATR examination of poly (acrylic acid) adsorbed onto hematite at low pH, Langmuir 19(14) (2003) 5802-5807.

[39] S. van Berkum, J.T. Dee, A.P. Philipse, B.H. Erné, frequency-dependent magnetic susceptibility of magnetite and cobalt ferrite nanoparticles embedded in PAA hydrogel, International journal of molecular sciences 14(5) (2013) 10162-10177.

[40] M. Moharram, M.A. Allam, Study of the interaction of poly (acrylic acid) and poly (acrylic acid□poly acrylamide) complex with bone powders and hydroxyapatite by using TGA and DSC, Journal of applied polymer science 105(6) (2007) 3220-3227.

[41] M.R. Alexander, S. Payan, T.M. Duc, Interfacial interactions of plasma-polymerized acrylic acid and an oxidized aluminium surface investigated using XPS, FTIR and poly(acrylic acid) as a model compound, Surface and Interface Analysis 26(13) (1998) 961-973.

[42] E. Atanassova, T. Dimitrova, J. Koprinarova, AES and XPS study of thin RF-sputtered Ta2O5 layers, Applied Surface Science 84(2) (1995) 193-202.

[43] Y.-C. Lu, C.-X. Yang, X.-P. Yan, Radiopaque tantalum oxide coated persistent luminescent nanoparticles as multimodal probes for in vivo near-infrared luminescence and computed tomography bioimaging, Nanoscale 7(42) (2015) 17929-17937.

[44] P.A. Jackson, W.N.W.A. Rahman, C.J. Wong, T. Ackerly, M. Geso, Potential dependent superiority of gold nanoparticles in comparison to iodinated contrast agents, European journal of radiology 75(1) (2010) 104-109.

[45] Y. Huang, H. Yu, C. Xiao, pH-sensitive cationic guar gum/poly (acrylic acid) polyelectrolyte hydrogels: Swelling and in vitro drug release, Carbohydrate Polymers 69(4) (2007) 774-783.

[46] J. Ricka, T. Tanaka, Swelling of ionic gels: quantitative performance of the Donnan theory, Macromolecules 17(12) (1984) 2916-2921.

[47] L. Serra, J. Doménech, N.A. Peppas, Drug transport mechanisms and release kinetics from molecularly designed poly (acrylic acid-g-ethylene glycol) hydrogels, Biomaterials 27(31) (2006) 5440-5451.

[48] C.D. Modi, S.J. Patel, A.B. Desai, R. Murthy, Functionalization and evaluation of PEGylated Carbon Nanotubes as novel Drug delivery for methotrexate, Journal of Applied Pharmaceutical Science 01(5) (2011) 103-108.

[49] R. Omidirad, F.H. Rajabi, B.V. Farahani, Preparation and in vitro drug delivery response of doxorubicin loaded PAA coated magnetite nanoparticles, Journal of the Serbian Chemical Society 78(10) (2013) 1609-1616.

[50] M. Alvarez-Figueroa, M.B. Delgado-Charro, J. Blanco-Mendez, Passive and iontophoretic transdermal penetration of methotrexate, International journal of pharmaceutics 212(1) (2001) 101-107.

[51] A. Göpferich, Mechanisms of polymer degradation and erosion, The Biomaterials: Silver Jubilee Compendium, Elsevier2006, pp. 117-128.

[52] R. Jerome, R. Forte, S. Varshney, R. Fayt, P. Teyssie, The anionic polymerization of alkyl acrylates: A challenge, Recent Advances in Mechanistic and Synthetic Aspects of Polymerization, Springer1987, pp. 101-117.